Hindawi
Advances in Materials Science and Engineering
Volume 2019, Article ID 9147849, 9 pages
https://doi.org/10.1155/2019/9147849

Research Article

Transverse Deformations and Structural Phenomenon as Indicators of Steel Fibred High-Strength Concrete Nonlinear Behavior

Iakov Iskhakov and Yuri Ribakov

Department of Civil Engineering, Ariel University, Ariel 40700, Israel

Correspondence should be addressed to Yuri Ribakov; ribakov@ariel.ac.il

Received 20 January 2019; Accepted 12 February 2019; Published 5 March 2019

Guest Editor: Young H. Kim

As known, high-strength compressed concrete elements have brittle behavior, and elastic-plastic deformations do not appear practically up to their ultimate limit state (ULS). This problem is solved in modern practice by adding fibers that allow development of nonlinear deformations in such elements. As a rule, are applied steel fibers that proved high efficiency and contribute ductile behavior of compressed high-strength concrete (HSC) elements as well as the desired effect at long-term loading (for other types of fibers, the second problem is still not enough investigated). However, accurate prediction of the ULS for abovementioned compression elements is still very important and current. With this aim, it is proposed to use transverse deformations in HSC to analyze compression elements' behavior at stages close to ultimate. It is shown that, until the appearance of nonlinear transverse deformations (cracks formation), these deformations are about 5-6 times lower than the longitudinal ones. When cracks appear, the tensile stress-strain relationship in the transverse direction becomes nonlinear. This fact enables to predict that the longitudinal deformations approach the ultimate value. Laboratory tests were carried out on 21 cylindrical HSC specimens with various steel fibers content (0, 20, 30, 40, and 60 kg/m^3). As a result, dependences of transverse deformations on longitudinal ones were obtained. These dependences previously proposed by the authors' concept of the structural phenomenon allow proper estimation of the compressed HSC state up to failure. Good agreement between experimental and theoretical results forms a basis for further development of modern steel fibered HSC theory and first of all nonlinear behavior of HSC.

1. Introduction

The first experimental study on Poisson's ratio (relation between transverse and longitudinal deformations before the appearance of transverse cracks) was carried out more than 100 years ago and was associated with plain and reinforced concrete columns [1, 2]. During the last century, the issue of Poisson's deformations was widely investigated. To obtain Poisson's ratios related to cylinder strength and age, 58 specimens were tested [3]. Corresponding theory was developed. It was concluded that there is no experimental evidence relating Poisson's coefficient of concrete to its strength. At the same time, our experimental results demonstrate that this ratio grows after the appearance of transverse cracks [4]. However, in this case, it is not Poisson's coefficient, but a ratio between transverse and longitudinal deformations.

An experimental study on the influence of stirrup and steel fiber reinforcement on the strength and deformation characteristics of conventionally reinforced $150 \times 150 \times 750$ mm concrete columns was carried out [5]. Steel fibers ratios were between 0 and 3% of the total composite material volume. It was reported that the column specimens had an increased energy absorption, high lateral strain, and greater Poisson's coefficient. The strength of the compression members is unaffected by either steel fiber volume or stirrup spacing.

Steel fibered high-strength concrete (SFHSC) became in the recent decades a very popular material in structural engineering [6]. As a result of increased application of SFHSC, many experimental studies are conducted to investigate its properties and to develop new rules for proper design. One of the trends in SFHSC structures is to provide their ductile behavior that is desired for proper structural

response to dynamic loadings. Review of recent experimental results obtained in the field of SFHSC is presented, and possible ways for developing modern design techniques for SFHSC structures are given.

Experimental studies were carried out to select effective fiber contents as well as suitable fiber types, to study most efficient combination of fiber and regular steel bar reinforcement [4]. It was shown that steel fibers have little effect on beams' elastic deformations but increase the ultimate ones, due to additional energy dissipation potential of steel fibers. This effect was further studied in repaired bending elements (two-layer beams) [7, 8]. It was shown that combination of the normal strength concrete layer with SFHSC one leads to effective and low-cost solution that may be used in new structures and for retrofitting existing ones.

Effect of steel fibers on postcracking and fracture behavior of concrete was also recently studied [9]. Plain and fiberd concrete specimens were tested. The strength properties, crack opening displacement, postcracking, and fracture behavior were studied. In our opinion, investigating postcracking behavior of concrete is interesting also from the viewpoint of transverse deformations, which will be discussed in the present paper.

Model fracture parameters of steel fiberd self-compacting concrete were derived from numerical simulation of splitting tensile tests [10]. The research allowed a comparison between the stress-crack width relationship from the tests and from analysis. For this purpose, a comprehensive nonlinear three-dimensional finite element modeling strategy was developed. The postcracking tensile laws, obtained from the modeling, provided a relationship with those obtained from the tests. In our opinion, analysis of stress-crack relationship of such concrete elements from the viewpoint of transverse deformations is also important, as it will allow more deeper understanding of SFHSC compressed elements' behavior.

Analytical and experimental results were presented for flexural response of SFRC beams [11]. Steel fiber content of 0.0%, 0.5%, 1.0%, and 2.0% by volume was used. Compressive strength and elastic modulus showed negligible changes with the inclusion of steel fibers, while the strain capacity and postpeak behavior were improved. Addition of more than 1.0% of steel fibers (by volume) resulted in significant improvement of flexural strength, deflection capacity, and postpeak ductility. The fracture energy increased with the increase in the fiber content. The authors have previously shown that the total energy dissipation during a loading-unloading cycle increases up to the fiber weight ratio (FWR) = 30 kg/m^3, that is, about 1.2% by volume [4]. Increasing the FWR to 40 kg/m^3 (about 1.6% by volume) yields almost the same energy dissipation, but further increase in FWR causes strong decreasing in dissipated energy.

Poisson's effect of concrete with lightweight aggregate was investigated [12]. The reduction of peak stress and modulus of elasticity was observed with increase of the volume fraction of shale aggregate. From the ratio of the lateral strain to the axial one, a more significant Poisson's effect was viewed for the concrete with a higher content of the shale aggregate. A corresponding expression was proposed to calculate the lightweight concrete stress-strain relation. Longitudinal and transverse deformations were measured and plotted. Following the experimental stress-strain curve results, the maximum deformations in longitudinal and transverse directions are about 2.3‰ and 0.5‰, respectively. It should be mentioned that the ratio between these values is about 5 times, which is well known from the existing design codes. Therefore, this ratio should be studied for fibred and nonfibred high-strength concrete, which will be done in the present study.

2. High-Strength Concrete and Its Application Problems

In the last decades, high-strength concrete (HSC) became a widely used construction material. During this period, a definition of HSC was given [13]. The modern codes for design of reinforced concrete (RC) structures included HSC up to concrete class C 90 [14]. As a rule, HSC is used with fibers. For example, a review of steel fibered HSC applications has been performed [6]. Optimal content of steel fibers for such concrete was obtained [4, 15]. Figure 1 shows the plastic energy dissipation in HSC specimens, U, and the fibers' weight ratios, FWR. As it follows from Figure 1, increasing the steel fibers' content from 0 to 30–40 kg/m^3 yields an increase in the dissipated energy, and further increasing of FWR above 40 kg/m^3 yields a decrease in energy dissipation. Thus, the reviled optimal steel fiber ratio for HSC is 30–40 kg/m^3. This result was obtained, based on experimental investigation of 21 standard cylindrical specimens with FWR of 0, 20, 30, 40, and 60 kg/m^3 [4].

As known, HSC is a brittle material. For example, the stress-strain graph for concrete class C 90 according to [14] corresponds to a parabola with an exponent of 1.4 and has no descending branch (Figure 2 and Table 1). Comparison of the graphs for concrete classes C 90, C 70, and C 50 shows that plastic energy dissipation decreases for class C 70, compared to C 50, and remains almost constant for concrete class C 90. Therefore, C 70 is defined as the lowest HSC class [13]. As it is evident from Table 1, the total energy dissipation in HSC is almost twice lower than in normal-strength concrete (NSC).

Using steel fibers in HSC increase the plastic deformations almost twice, but just at the stage that is close to the concrete ultimate state [7]. Therefore, in spite of adding fibers, it is impossible to know the compressed concrete section state: elastic, elastic-plastic, or plastic. Hence, the aim of the present paper is to find alternative methods to solve the problem.

3. Essence of Structural Phenomenon

Many researchers have investigated the behavior of structures under loads that increase from the elastic state up to failure. In this case, following the results obtained by the authors [16], if a structure and the load are symmetric, usually structural parameters in the elastic state increase or decrease twice at failure. We have called such changes in parameters of a structure as "structural phenomenon". This

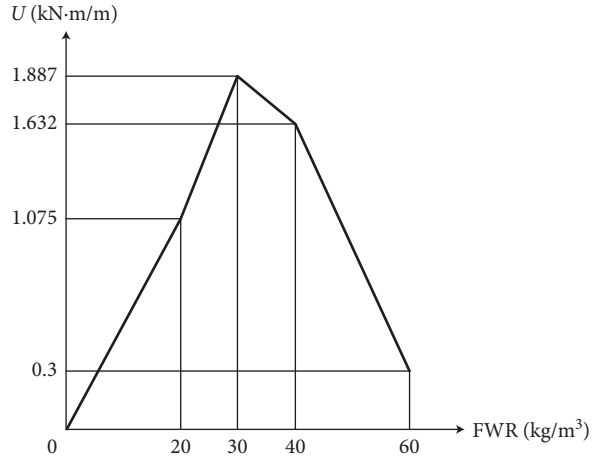

Figure 1: Energy dissipated during loading and unloading for cylindrical specimens with different FWRs [4].

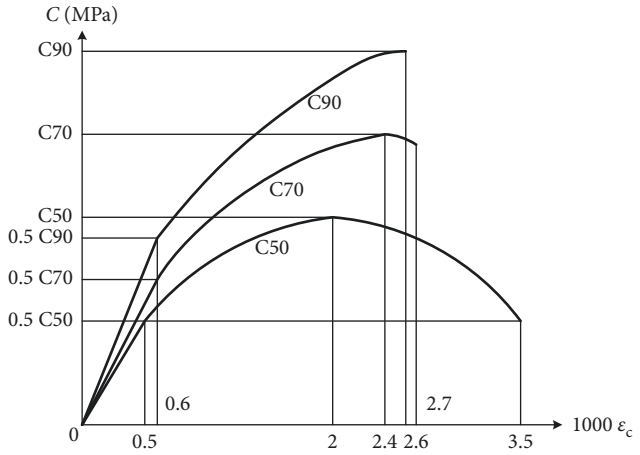

Figure 2: Stress-strain relationships for concrete classes C 50 (normal-strength concrete), C 70 (the lowest limit strength of high-strength concrete), and C 90 (high-strength concrete) [13].

phenomenon was analyzed for the following groups of experiments:

(i) Investigation of structural concrete at the material level

(ii) Behavior of RC structures and elements under static loads

(iii) Response of RC structures and elements to dynamic loads

The phenomenon is based on two fundamental ideas:

(i) Quasi-isotropic state of a structure at the ultimate limit state (ULS) [17]

(ii) Mini-max principle [18]

Moreover, the phenomenon provides valuable indicators for experiments planning, estimation of the structural state (elastic, elastic-plastic, plastic, or failure), etc.

From the mathematical viewpoint, the phenomenon provides additional equation(s) that enable to calculate parameters, usually obtained experimentally or using some coefficients. Therefore, using this phenomenon can lead to developing proper design concepts and new RC theory, in which the number of empirical design coefficients will be minimal.

Table 1: Energy dissipation comparison for concrete classes C 50, C 70, and C 90.

Energy dissipation from the graph $\sigma_c - \varepsilon_c$	Concrete class according to Eurocode 2		
	C 50	C 70	C 90
Graph exponent, n	2	1.45	1.4
Descending branch	Yes	No	No
Ratio between the area of the parabola to that of the described rectangle, $n/(n+1)$	0.667	0.592	0.584
Elastic energy dissipation, E_{el}	0.125 f_c (‰)	0.15 f_c (‰)	0.15 f_c (‰)
Plastic energy dissipation, E_{pl}	f_c (‰)	0.624 f_c (‰)	0.642 f_c (‰)
Total energy dissipation, E_{tot}	1.125 f_c (‰)	1.216 f_c (‰)	1.236 f_c (‰)
Ductility coefficient, E_{tot}/E_{el}	9.00	8.10	8.24

The above-described features of structural phenomenon enable to use it in the frame of the present study for obtaining a theoretical stress-strain curve of concrete. This approach is useful for many design aspects, including calculating the values of concrete elements ductility for high- and normal-strength concrete with and without fibers, which are usually obtained experimentally or using empirical dependences [19].

4. Evaluation of Available Experimental Data

Many experimental investigations were focused on studying SFHSC properties using cylindrical specimens with different steel fiber contents [4, 20, 21]. Table 2 summarizes available data from testing 21 cylindrical specimens, reported in the abovementioned studies. At the first stage [4], five different steel fiber contents were used, and at further stages [20, 21], optimal FWR = 30 kg/m^3 was used to obtain strength and deformation properties of the investigated SFHSC.

Investigating the deformation properties is focused on transverse tensile deformations in the tested specimens vs. the longitudinal ones. According to the available standards [14, 22, 23] and publications [15, 24], there are some differences in concrete transverse tensile deformations ε_{trans}, ultimate tensile deformations $\varepsilon_{ct\ ul}$, and Poisson's coefficient μ_c (Table 3). Therefore, the present study is based on available experimental data (Table 4).

Following this table, transverse tensile deformations are divided into two stages:

(i) Before the appearance of transverse cracks ($\varepsilon_{trans} \leq \varepsilon_{ct\ ul}$)

(ii) After the appearance of transverse cracks and up to specimen's failure ($\varepsilon_{trans} > \varepsilon_{ct\ ul}$)

These two stages are evident, for example, in response of RC columns to strong earthquake in Mexico, 2017 (Figure 3)

Table 2: Available data from testing HSC cylindrical specimens.

Reference	Number of tested specimens	Compressive strength (MPa)	Fiber weight ratio (kg/m^3)	Modulus of elasticity (MPa)
Holschemacher et al. [4]	15	86–91	0, 20, 30, 40, 60	—
Iskhakov et al., [18]	3	90.5*	30	41603*
Iskhakov et al., [21]	3	79.5*	30	39134*

*Average values.

Table 3: Poisson's ratio, μ_c, and ultimate tensile deformations, $\varepsilon_{ct\ ul}$.

Pos. No.	References	μ_c	$\varepsilon_{ct\ ul}$ (‰)
1	SI 466 [23]	0.15–0.25 (average. 0.2)	—
2	Bondarenko and Suvorkin [24]	0.2	0.1–0.2 (average 0.15)
3	BR [22]	0.2	0.15
4	Eurocode 2 [14]	0.2	—
5	Iskhakov [15]	0.15–0.2	0.07–0.12

Table 4: Experimental values of Poisson's coefficients for concrete class C 90 (pos. 1) and relation between transverse and longitudinal deformations (pos. 2).

Pos. no.	Limits of transverse deformations	Fiber weight ratio (FWR) (kg/m^3)					Average	Average 2/Average 1
		0	20	30	40	60		
1	$\varepsilon_{trans} \leq \varepsilon_{ct\ ul}$	0.11	0.18	0.22	0.16	0.08	0.15	2.0
2	$\varepsilon_{trans} > \varepsilon_{ct\ ul}$	0.20	0.32	0.44	0.40	0.14	0.30	
3	Pos. 2/pos. 1	1.88	1.78	2.0	2.5	1.75	1.97	

(a) (b)

Figure 3: Transverse cracks in a column during Mexico earthquake 2017 [25]: (a) 2 sec. (b) 15 sec. 1: crack initiation; 2: crack development.

[25]. As it follows from Figure 3, a crack due to transverse deformations (transverse cracks) appear at the 2nd second of the earthquake. Opening of the crack is a process, in which it develops in the longitudinal and transverse direction of the column (compare Figures 3(a) and 3(b)).

It should be mentioned that for SFHSC transverse deformations increase at both of the abovementioned stages up to FWR = 30 kg/m^3 and decrease for a higher fiber content. The average transverse deformation at the first stage is 0.15, and at the second one, it is 0.30 (the value is increased twice), which corresponds to the structural phenomenon, proposed recently by the authors [16].

The abovementioned two stages have the following explanation: at ultimate longitudinal elastic deformations, $\varepsilon_c = 0.5$‰, and the transverse deformations $\varepsilon_{trans} \approx 0.1$‰, and it corresponds to concrete ultimate tensile deformations (Table 3). After that (at $\varepsilon_c > 0.5$‰), the transverse cracks opening process appears (Figure 4). At the same time, the second stage, according to the structural phenomenon, is divided into two subcases:

(i) cracks' development ($\varepsilon_{ct\ ul} < \varepsilon_{trans} \leq 2\ \varepsilon_{ct\ ul}$), corresponding to Figures 3(a) and 4(b)

(ii) failure ($\varepsilon_{trans} > 2\ \varepsilon_{ct\ ul}$), corresponding to Figures 3(b) and 4(c)

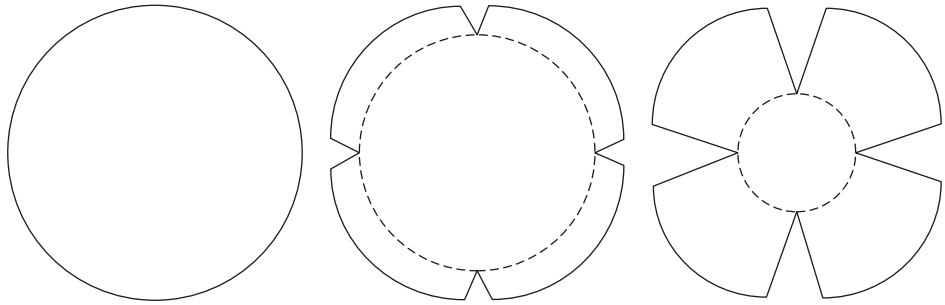

Figure 4: Development of transverse deformations and cracks at stages 1 (a) and 2 (b) for cylindrical HSC specimens.

5. Detailed Analysis and Theoretical Interpretation of Experimental Results

5.1. Dependence of Load vs. Longitudinal and Load vs. Transverse Deformations. For cylindrical HSC specimens without fibers (Figure 5(a)), the dependences between load and longitudinal deformations as well as that between load and transverse ones are linear up to the ultimate state. In this case, the transverse deformations are actually also the Poisson ones, as nonlinear behavior is practically not evident. The specimens' behavior up to failure corresponds to Figure 4(a), i.e., transverse cracks do not appear. Poisson's coefficient is about 0.2. Similar results were obtained for the three specimens that were tested. It should be mentioned that both longitudinal and transverse deformations sharply increase at the ultimate state, which is explained by the specimens' failure process.

At fiber content (FWR) of 20 kg/m^3, the longitudinal deformations remain practically linear up to failure, at which plastic deformations develop. However, transverse deformations exhibit nonlinear behavior from about 70% of concrete strength, i.e., in this case, Poisson's coefficient can be calculated before nonlinear deformations initiate. Initiation of transverse cracks corresponds to stage 2 (Figure 4(b)), i.e., the specimens are in the stage of transverse cracks' development ($\varepsilon_{ct\ ul} \leq . \varepsilon_{trans} \leq 2\ \varepsilon_{ct\ ul}$).

Increasing the FWR to 30 and 40 kg/m^3 leads to more evident nonelastic development of transverse deformations after reaching the limit tensile concrete deformations value $\varepsilon_{ct\ ul}$ (Figures 5(c) and 5(d)). Further increase in FWR to 60 kg/m^3 yields a decrease in development of transverse deformations (Figure 5(e)). Following Figure 5(e), appearance and development of transverse cracks is not reflected in longitudinal deformations, but it shows that a compressed element is at a state that is close to an ultimate one. This is the role of transverse deformations as an indirect indicator of compressed steel fibered concrete behavior.

5.2. Dependence of Transverse Deformations on Longitudinal Ones. As known, modern design codes operate with constant Poisson's ratios as relation between transverse and longitudinal deformations $\mu_c = \varepsilon_{trans}/\varepsilon_{long}$ (Table 3). For example, following [14], Poisson's ratio may be taken equal to 0.2 for uncracked concrete and 0 for cracked one.

At the same time, as shows the experimental data [4], after the elastic limit is over, transverse deformations do not become equal to zero but develop nonlinearly within the limits $\varepsilon_{ct\ ul} \leq . \varepsilon_{trans} \leq 2\ \varepsilon_{ct\ ul}$ (Figure 4(b) that corresponds to stage 2). This behavior satisfies the structural phenomenon concept. When ε_{trans} exceeds the value of 2 $\varepsilon_{ct\ ul}$ (Figure 4(c)), the longitudinal deformations are not limited and the element approaches failure. Thus, analysis of the HSC behavior, considering transverse deformations, allows predicting of all concrete stages, including its nonlinear performance. By the way, these stages are evident from behavior of a concrete building column during an earthquake (Figure 3).

The abovementioned ideas correspond to experimental data presented in Figure 6 that shows dependences of transverse deformations on longitudinal ones for various FWR values from 0 to 60 kg/m^3. Analysis of the graphs in Figure 6 shows (especially in the cases when FWR = 30–40 kg/m^3, corresponding to optimal fiber content, according to Figure 1) that there are three stages in concrete behavior:

(i) Linear
(ii) Nonlinear
(iii) Limit

It is evident from Figures 6(c) and 6(d) that, for $\varepsilon_{trans} \leq 0.2‰$, transverse deformations develop proportionally to longitudinal ones, which corresponds to Poisson's deformations. When $\varepsilon_{trans} > 0.2‰$, the graphs become nonlinear and the transverse deformations develop more intensively than longitudinal ones. For $\varepsilon_{trans} > 0.4‰$ (that corresponds to the value of 2 $\varepsilon_{ct\ ul}$), transverse deformations sharply increase.

Further theoretical interpretation of such behavior of SFHSC (dependence between $\varepsilon_{trans}/\varepsilon_{long}$ vs. ε_{long}) is presented in Figure 7. The main feature in SFHSC behavior (that is evident from Figure 7) is that for longitudinal deformations $\varepsilon_{long} \leq 1‰$ the ratio $\varepsilon_{trans}/\varepsilon_{long}$ is constant—it

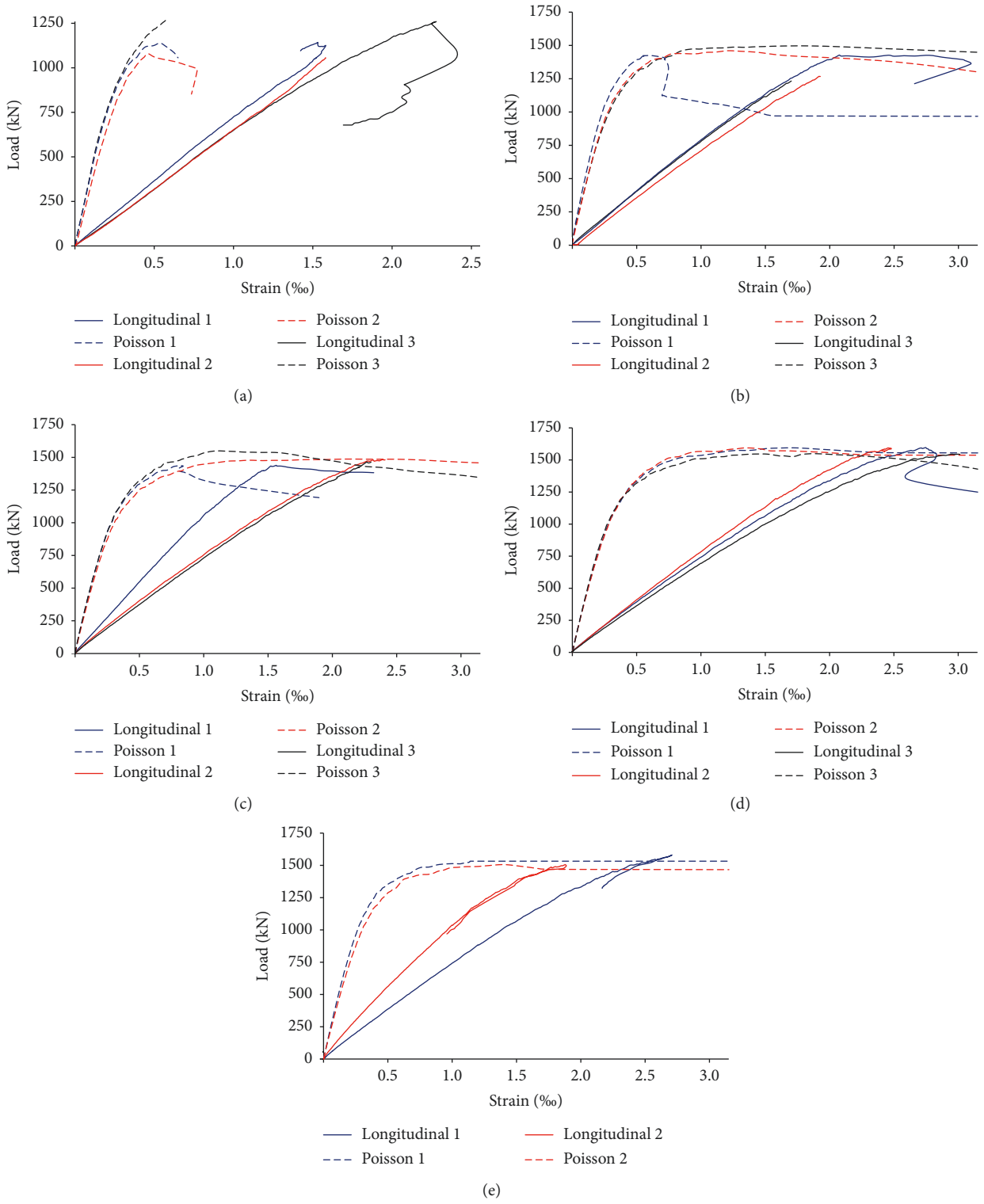

Figure 5: Load-strain diagrams for HSC with different FWRs. (a) FWR = 0; (b) FWR = 20 kg/m^3; (c) FWR = 30 kg/m^3; (d) FWR = 40 kg/m^3; (e) FWR = 60 kg/m^3.

indicates that the SFHSC behaves linearly. When 1‰ ≤ $\varepsilon_{long} \leq 2$‰, the SFHSC behaves nonlinearly, and for $\varepsilon_{long} > 2$‰, it approaches to failure.

The ratios between transverse and longitudinal deformations ($\varepsilon_{trans}/\varepsilon_{long}$) vs. the longitudinal ones (ε_{long}) are presented in Table 5. As listed in Table 5, higher longitudinal deformations correspond to higher $\varepsilon_{trans}/\varepsilon_{long}$ ratios. Relation between the measured deformations' values and those proposed in the theoretical interpretation are shown in Figure 8. The obtained result enables to revile the main

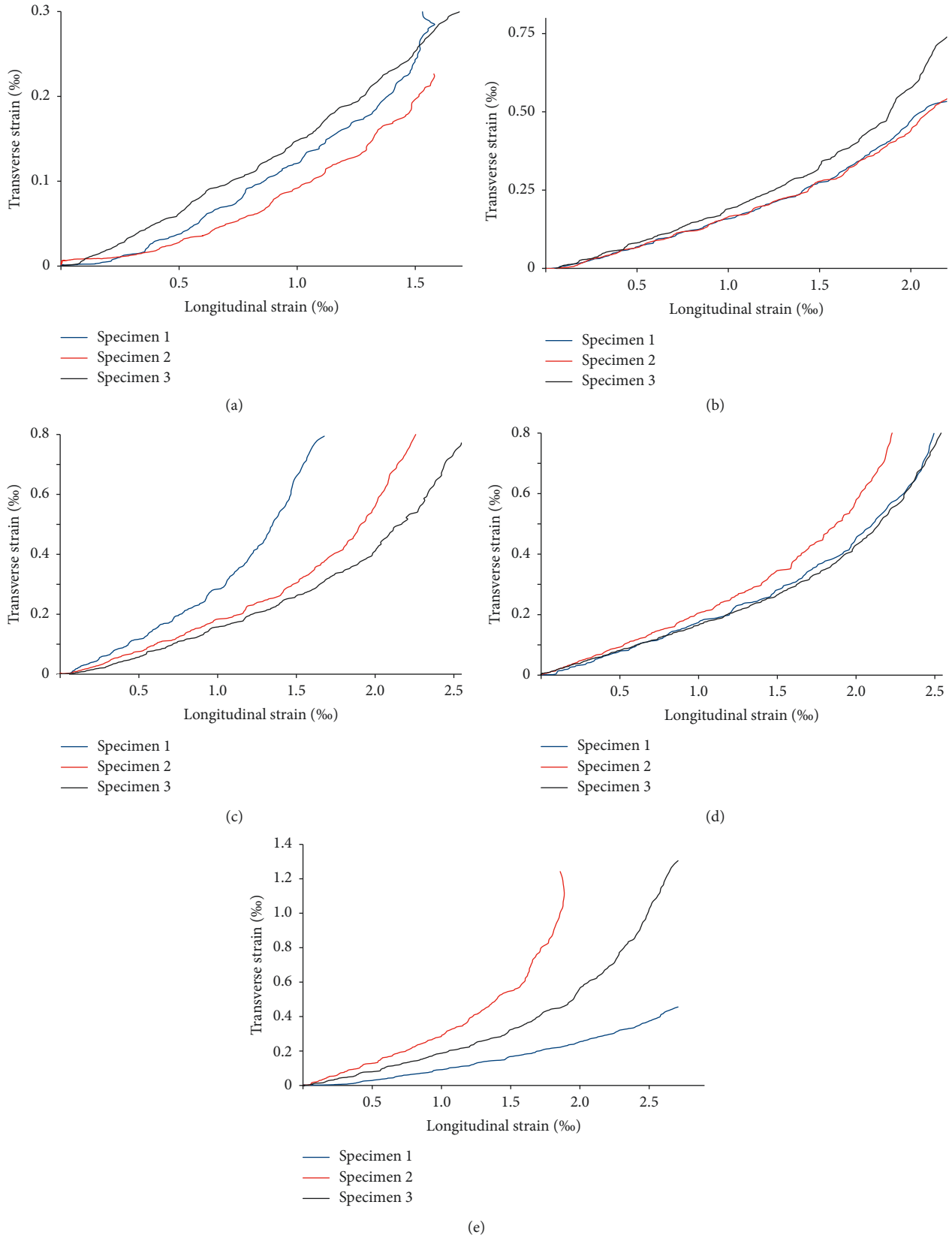

Figure 6: Dependence of transverse strain on longitudinal one for (a) FWR = 0; (b) FWR = 20 kg/m^3; (c) FWR = 30 kg/m^3; (d) FWR = 40 kg/m^3; (e) FWR = 60 kg/m^3.

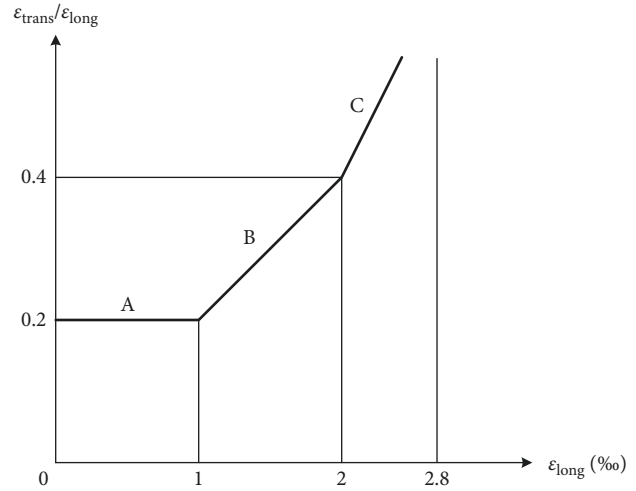

Figure 7: Proposed theoretical relationship between longitudinal deformations and transverse to longitudinal deformations' ratio: A, linear behavior of HSC; B, nonlinear behavior of HSC; C, stage before the HSC reaches the ULS.

Table 5: The ratio between transverse and longitudinal deformations ($\varepsilon_{trans}/\varepsilon_{long}$) vs. the longitudinal ones (ε_{long}).

FWR (kg/m^3)	Specimen	$\varepsilon_{trans}/\varepsilon_{long}$		
		$\varepsilon_{long} \leq 1‰$	$1‰ \leq \varepsilon_{long} \leq 2‰$	$\varepsilon_{long} \geq 2‰$
0	1	0.12	0.22	—
	2	0.09	0.17	—
	3	0.14	0.25	0.5
	Average	0.12	0.21	0.5
20	1	0.18	0.30	—
	2	0.18	0.30	0.52
	3	0.20	0.28	0.65
	Average	0.19	0.29	0.58
30	1	—	—	—
	2	0.20	0.3	0.60
	3	0.15	0.25	0.80
	Average	0.18	0.28	0.70
40	1	0.18	0.22	0.80
	2	0.20	0.40	1.00
	3	0.18	0.22	0.80
	Average	0.19	0.28	0.87
60	1	—	—	—
	2	0.25	0.75	2.00
	3	0.20	0.25	—
	Average	0.23	0.50	2.00

stages in SFHSC behavior, and therefore, it is useful for more effective design of SFHSC elements.

It should be highlighted that the abovementioned analysis became possible due to application of the structural phenomenon concept, explained in Section 3.

6. Conclusions

Accurate prediction of nonlinear behavior of compressed steel fibered high-strength concrete (SFHSC) elements is investigated experimentally and theoretically. For the first time, development of nonlinear postcracking transverse deformations was used to analyze nonlinear behavior of SFHSC compressed elements.

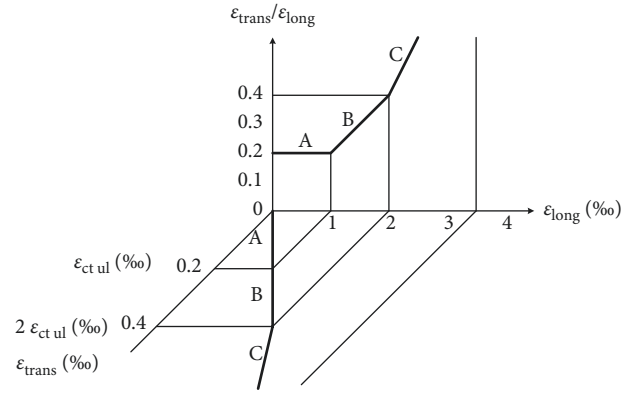

Figure 8: Theoretical dependences between transverse deformations vs. longitudinal deformations and transverse to longitudinal deformations' ratio vs. longitudinal deformations: A, linear behavior of HSC; B, nonlinear behavior of HSC; C, stage before the HSC reaches the ULS.

Using the structural phenomenon enables to revile three stages of transverse deformations' development in compressed SFHSC elements: linear ($\varepsilon_{trans} \leq \varepsilon_{ct\ ul}$), nonlinear ($\varepsilon_{ct\ ul} \leq \varepsilon_{trans} \leq 2\ \varepsilon_{ct\ ul}$), and ultimate ($\varepsilon_{trans} > 2\ \varepsilon_{ct\ ul}$).

Unlike in current normative documents, the physical meaning of Poisson's coefficient is expanded for cases, when transverse cracks appear in compressed concrete elements. It is shown that, at optimal fiber content, this coefficient increases up to twice, which completely corresponds to the structural phenomenon.

Dependences of transverse deformations on longitudinal ones were obtained experimentally and theoretically. These dependences previously proposed by the authors concept of the structural phenomenon allow proper estimation of compressed SFHSC states, including nonlinear behavior, up to failure.

Good agreement between experimental and theoretical results forms a basis for further development of modern steel fibered HSC theory (and first of all nonlinear behavior of SFHSC) that can be applied in modern design codes.

Data Availability

All required data are included in the manuscript.

Conflicts of Interest

The authors declare that there no conflicts of interest regarding the publication of this paper.

References

[1] A. N. Talbot, *Tests of Concrete and Reinforced Concrete Columns, Engineering Experiment Station*, University of Illinois, Bulletin No. 20, 1907.

[2] M. O. Withey, *Tests of ReinJorced Concrete Columns*, University of Wisconsin, Bulletin No. 466, 1911.

[3] A. E. Allos and L. H. Martin, "Factors affecting Poisson's ratio for concrete," *Building and Environment*, vol. 16, no. 1, pp. 1–9, 1981.

[4] K. Holschemacher, I. Iskhakov, Y. Ribakov, and T. Mueller, "Laboratory tests of two-layer beams consisting of normal and fibered high strength concrete: ductility and technological aspects," *Mechanics of Advanced Materials and Structures*, vol. 19, no. 7, pp. 513–522, 2012.

[5] P. S. Mangat and M. Motamedi Azari, "Influence of steel fibre and stirrup reinforcement on the properties of concrete in compression members," *International Journal of Cement Composites and Lightweight Concrete*, vol. 7, no. 3, pp. 183–192, 1985.

[6] A. A. Shah and Y. Ribakov, "Recent trends in steel fibered high-strength concrete," *Materials & Design*, vol. 32, no. 8-9, pp. 4122–4151, 2011.

[7] I. Iskhakov and Y. Ribakov, "A new concept for design of fibered high strength reinforced concrete elements using ultimate limit state method," *Materials & Design*, vol. 51, pp. 612–619, 2013.

[8] I. Iskhakov, Y. Ribakov, K. Holschemacher, and T. Mueller, "High performance repairing of reinforced concrete structures," *Materials & Design*, vol. 44, pp. 216–222, 2013.

[9] F. Bencardino, L. Rizzuti, G. Spadea, and R. N. Swamy, "Implications of test methodology on post-cracking and fracture behaviour of Steel Fibre Reinforced Concrete," *Composites Part B: Engineering*, vol. 46, pp. 31–38, 2013.

[10] A. Abrishambaf, J. A. O. Barros, and V. M. C. F. Cunha, "Tensile stress-crack width law for steel fibre reinforced self-compacting concrete obtained from indirect (splitting) tensile tests," *Cement and Concrete Composites*, vol. 57, pp. 153–165, 2015.

[11] D.-Y. Yoo, Y.-S. Yoon, and N. Banthia, "Predicting the post-cracking behavior of normal- and high-strength steel-fiber-reinforced concrete beams," *Construction and Building Materials*, vol. 93, pp. 477–485, 2015.

[12] B. Han and T.-Y. Xiang, "Axial compressive stress-strain relation and Poisson effect of structural lightweight aggregate concrete," *Construction and Building Materials*, vol. 146, pp. 338–343, 2017.

[13] I. Iskhakov and Y. Ribakov, "A design method for two-layer beams consisting of normal and fibered high strength concrete," *Materials & Design*, vol. 28, no. 5, pp. 1672–1677, 2007.

[14] *Eurocode 2: Design of Concrete Structures–Part 1-1: General Rules and Rules for Buildings*, 2004.

[15] I. Iskhakov, *Plastic Energy Dissipation, Ductility and Load-Carrying Capacity of RC Elements*, ALFA Publishers, 2012, in Hebrew

[16] I. Iskhakov and Y. Ribakov, "Structural phenomenon of cement-based composite elements in ultimate limit state," *Advances in Building Technologies and Construction Materials*, Article ID 4710752, 9 pages, 2016.

[17] I. Iskhakov, "Quasi-isotropic ideally elastic-plastic model for calculation of RC elements without empirical coefficients," in *Structural Engineering, Mechanics and Computation*, Vol. 1, A. Zingoni, Ed., Elsevier Press, Cape Town, South Africa, 2001.

[18] I. Iskhakov and Y. Ribakov, *Ultimate Equilibrium of RC Structures using Mini-Max Principle*, Nova Science Publishers, Inc., Hauppauge, NY, USA, 2014.

[19] I. Iskhakov, Y. Ribakov, and A. Shah, "Experimental and theoretical investigation of column - flat slab joint ductility," *Materials & Design*, vol. 30, no. 8, pp. 3158–3164, 2009.

[20] I. Iskhakov, Y. Ribakov, K. Holschemacher, and T. Mueller, "Experimental investigation of full scale two-layer reinforced concrete beams," *Mechanics of Advanced Materials and Structures*, vol. 21, no. 4, pp. 273–283, 2014.

[21] I. Iskhakov, Y. Ribakov, and K. Holschemacher, "Experimental investigation of continuous two-layer reinforced concrete beams," *Structural Concrete*, vol. 18, no. 1, pp. 205–215, 2017.

[22] *BR 52-101-2003, Non-pre-stressed concrete and reinforced concrete structures*, NIIZhB, Moscow, 2004, in Russian.

[23] *SI 466 Concrete code: General principles, part 1*, The Standards Institution of Israel, 2012.

[24] V. M. Bondarenko and D. G. Suvorkin, *Reinforced Concrete and Stone Structures*, Vysshaya Shkola, Moscow, 1987, in Russian.

[25] *Mexico earthquake September 2017*, 2018, https://twitter.com/nssoaxaca/status/910224886014136320?refsrc=twsrc%5Etfw%7Ctwcamp%5Etweetembed%7Ctwterm%5E910224886014136320&ref_url=https%3A%2F%2Fwww.businessinsider.com%2Fmexico-puebla-earthquake-photos-videos-twitter-facebook-2017-9.